Journal of Solid State Chemistry 181 (2008) 1361–1366

Contents lists available at ScienceDirect

Journal of Solid State Chemistry

journal homepage: www.elsevier.com/locate/jssc

Photocatalytic degradation of organic dyes on visible-light responsive photocatalyst $PbBiO_2Br$

Zhichao Shan [a,b], Wendeng Wang [a], Xinping Lin [a], Hanming Ding [b,*], Fuqiang Huang [a,*]

[a] State Key Laboratory of High Performance Ceramics and Superfine Microstructures, Shanghai Institute of Ceramics, Chinese Academy of Sciences, Shanghai 200050, PR China
[b] Department of Chemistry, East China Normal University, Shanghai 200062, PR China

ARTICLE INFO

Article history:
Received 2 January 2008
Received in revised form
6 March 2008
Accepted 9 March 2008
Available online 16 March 2008

Keywords:
Photocatalyst
$PbBiO_2Br$
Dye

ABSTRACT

The layered compound of lead bismuth oxybromide $PbBiO_2Br$, prepared by conventional solid-state reaction method, has an optical band gap of 2.3 eV, and possesses a good visible-light-response ability. The references, $PbBi_2Nb_2O_9$, $TiO_{2-x}N_x$, BiOBr and $BiOI_{0.8}Cl_{0.2}$, which are excellent visible-light-response photocatalysts, were applied to comparatively understand the activity of $PbBiO_2Br$. Degradation of methyl orange and methylene blue was used to evaluate photocatalytic activity. The results show that $PbBiO_2Br$ is more photocatalytically active than $PbBi_2Nb_2O_9$, $TiO_{2-x}N_x$ and BiOBr under visible light.

1. Introduction

The success in the development of photocatalysts in the past decades suggests their indispensable role in the range of solar energy utilization for hydrogen production and environment-organic-pollutant purification [1–7]. The initial step of the photocatalytic process consists of the generation of electron–hole pair upon irradiation of a photon whose energy is equal to or higher than that of the band gap (E_g) of a photocatalyst. The photoinduced electron–hole pairs can either recombine in the bulk or travel up to the surface, and the separated electrons or holes at surfaces can participate in chemical reactions with species adsorbed on the semiconductors surface.

Recently, layered structure compounds were found to promote the generation and the separation of the charge carriers and can be used as efficient photocatalysts for water splitting and degradation of pollutants under light irradiation because of their possibility of modifying chemical composition as well as microstructure by means of ionexchange, intercalation, or pillaring, which is useful for designing novel photocatalysts based on semiconducting metal oxide sheets. The typical layered photocatalysts are $AgInW_2O_8$ ($E_g = 3.12$ eV), $RbLnTa_2O_7$ (Ln = La, Pr, Nd, and Sm) ($E_g = 3.5$–3.9 eV), $Ln_2Ti_2O_7$ (Ln = La, Pr, Nd) ($E_g = 2.99$–3.82 eV), $AgAlO_2$ ($E_g = 2.8$ eV), $K_2Sr_{1.5}Ta_3O_{10}$ ($E_g = 4.1$ eV), $InTaO_4$ ($E_g = 3.7$ eV), etc. [8–13]. These semiconductors are good candidates for environmental remediation and water purification owing to their photoactivities toward degrading organic pollutants upon excitation with ultraviolet (UV) light. Some of them are even better than anatase TiO_2 or P25. However, most of the photocatalysts mentioned above [8–13] only respond to the UV light. The remarkable progress of the past years in photocatalysis has been limited to UV light instead of the visible light region. The development of visible-light photocatalysts has become one of the most important topics in photocatalysis.

In our previous work, we for the first time found that the layered nano-sized oxyhalide photocatalyst BiOCl [14] showed a higher photocatalytic activity to degrade methyl orange (MO) compared with P25 (TiO_2). Whereas, due to its wide optical bandgap (3.5 eV), BiOCl can also only absorb UV light. Recent efforts have been also carried out on the other layered nano-sized oxyhalides, such as BiOBr, $BiOI_xBr_{1-x}$, $BiOI_xCl_{1-x}$ [15,16], which possess good visible-light-response abilities. The internal electric fields in layered materials are considered to favor charge separation, which can subsequently induce redox reactions on the semiconductor surface and contribute to enhance the photocatalytic activity [17,18]. For example, in the bismuth oxyhalide semiconductor, the $[Bi_2O_2]$ and $[X_2]$ slices (X = Cl, Br, I) are one by one orderly stacked to form the unique layered structure. The permanent static electric fields between $[Bi_2O_2]$ and $[X_2]$ layers can work as accelerators for the separations of electron–hole pairs upon photoexcitation to favor a high photocatalytic efficiency of BiOX.

Herein, we report another novel layered photocatalyst $PbBiO_2Br$. The layered photocatalyst BiOBr has a band gap of

* Corresponding authors. Fax: +86 21 5241 3903.
E-mail addresses: hmding@chem.ecnu.edu.cn (H. Ding), huangfq@mail.sic.ac.cn (F. Huang).

0022-4596/$ - see front matter © 2008 Elsevier Inc. All rights reserved.
doi:10.1016/j.jssc.2008.03.001

2.9 eV, and the abundant solar energy can be utilized little due to its inherent limitation. It has been reported that many semiconductors containing a hybridized band structure often reveal the suitable band structure responsive to visible-light irradiation. For example, the high activity for photocatalytic H_2 and O_2 evolution on $AgNbO_3$ is attributed to the hybridized valence band of Ag 4*d* and O 2*p* [19], as well as O_2 evolution on $PbBi_2Nb_2O_9$ or $BiVO_4$ to the hybridized valence band of Bi 6*s* and O 2*p* [20,21]. In order to narrow the band gap of BiOBr and enhance the visible-light-driven ability of the photocatalyst, we incorporated Pb^{2+} into $[Bi_2O_2]$ layers based on the structure of BiOBr to form the derived compound of $PbBiO_2Br$. $PbBiO_2Br$ is expected to show a narrower band gap than BiOBr. Because the contribution of Pb $6s^2$ orbitals occupy higher energy states at the valence band maximum (VBM), and the contribution of Pb 6*p* orbitals occupy lower energy states at the conduction band minimum (CBM). The hybridized states of VBM and CBM can decrease the effective masses of holes and electrons, respectively, to favor a longer traveling distance for excited carriers. Just as expected, the experimentally estimated band gap of micro-metered $PbBiO_2Br$ (2.3 eV) is much narrower than that of nano-metered BiOBr (2.9 eV). Furthermore, the visible-light-response photocatalytic activity of the material is also higher than that of BiOBr. In our opinion, the higher activity for photocatalytic degradation of organic dyes on $PbBiO_2Br$ is not only attributed to the layered structure but also the hybridized band structure.

In this work, the references, $PbBi_2Nb_2O_9$ [20], $TiO_{2-x}N_x$ [22], BiOBr and $BiOI_{0.8}Cl_{0.2}$ [15,16], which possess an excellent performance to photocatalytically decompose organic pollutants or split water ($PbBi_2Nb_2O_9$) under visible light, were applied to comparatively understand the activity of $PbBiO_2Br$. Two representative organic dyes in the textile effluents, methylene blue (MB) and MO, were used as model contaminants for the purpose of photocatalytic activity evaluation [14,23–25]. The photodegradation of MO and MB over $PbBiO_2Br$ and the references $PbBi_2Nb_2O_9$, $TiO_{2-x}N_x$, BiOBr, and $BiOI_{0.8}Cl_{0.2}$, were investigated under both visible light and UV light irradiation.

2. Experiment

The crystalline $PbBiO_2Br$ powders were synthesized by a solid-state reaction method. BiOBr and PbO (AR, 99.5%) were used as raw materials. BiOBr was prepared by a soft chemical method described elsewhere [15,16]. A total of 0.02 mol $Bi(NO_3)_3 \cdot 5H_2O$ (AR, 99.0%) powders were dissolved in 15 mL glacial acetic acid (AR, 99.5%) in a water bath at 70 °C. Then the solution was added rapidly to 240 mL aqueous solution containing 0.04 mol sodium acetate (AR, 99.0%) and a stoichiometric amount of KBr (AR, 99.0%). The mixture was vigorously stirred for 20 h. After the reaction was completed, the resulting solid product was collected by filtration, washed three times with deionized water and then dried at 80 °C in a vacuum oven. During the synthesis of $PbBiO_2Br$, the well-mixed powders of BiOBr and PbO with the stoichiometric proportion were calcined at 700 °C for 20 h in an alumina crucible in air, with intermediate grindings.

The $BiOI_{0.8}Cl_{0.2}$ compound was also prepared by a soft chemical method [16]. The $Bi(NO_3)_3 \cdot 5H_2O$ (AR, 99.0%) powders were added slowly into an aqueous solution containing stoichiometric amounts of KCl (AR, 99.5%) and KI (AR, 99.5%). The mixture was adjusted to pH = 3 by using diluted NH_4OH solution and stirred vigorously for 24 h before the collected powders were collected, washed and dried.

The photocatalyst $PbBi_2Nb_2O_9$ was synthesized by the solid-state reaction of PbO (AR, 99.5%), Bi_2O_3 (AR, 99.5%), and Nb_2O_5 (AR, 99.5%) at 1100 °C for 10 h [20].

$TiO_{2-x}N_x$ powder samples were prepared by treating anatase TiO_2 powder at the atmosphere of NH_3:Ar (the flowing rates = 1:3) at 600 °C for 3 h [22].

The pure $PbBiO_2Br$, BiOBr, $BiOI_{0.8}Cl_{0.2}$, $PbBi_2Nb_2O_9$, and $TiO_{2-x}N_x$ phases were all confirmed by X-ray diffraction analysis (Bruker D8 Advance diffractometer using CuK_α radiation ($\lambda = 0.15406$ nm)). The optical band gap was estimated from the UV–vis (HITACHI U-3010 spectrophotometer) diffuse reflectance spectrum. The semiconductor absorption edge (λ_g) was determined by the linear extrapolation of the steep part of UV–vis light absorption toward the baseline [26,27]. While the band gap is estimated by the formula $\lambda_g\,(\text{nm}) = 1240/E_g\,(\text{eV})$.

Field-emission scanning electron microscopy (FE-SEM) images of the samples were obtained on a JSM-6700F field-emission scanning electron microscope.

The optical system for the catalytic reaction under visible light includes a 300 W Xe arc lamp, a reaction container, and a cut-off filter ($\lambda > 420$ nm). The Xe arc lamp is appended above the container with a distance of about 15 cm. In all the experiments, the reaction temperature was kept at room temperature to prevent any thermal catalytic effect by using the circulating water jack. The volume of initial MO or MB solution, with the concentration of 10 mg/L, was 200 mL. The powder concentration in the MO or MB aqueous solution was 0.20 g/100 mL. Visible light illumination was conducted after the suspension was strongly magnetically stirred in the dark for 60 min to reach the adsorption–desorption equilibrium of MO or MB on catalyst surfaces. During irradiation, about 3 mL suspension was continually taken from the reaction cell at given time intervals for subsequent MO or MB concentration analysis after centrifuging by measuring its maximum absorption with a UV–vis spectrophotometer (HITACHI U-3010 spectrophotometer). The dyes' degradation was calculated by the following equation:

$$\eta = (C_0 - C)/C_0 = (A_0 - A)/A_0 \quad (1)$$

where C_0 and A_0 are the initial concentration after equilibrium adsorption and absorbance of MO/MB solution at 464/664 nm corresponding to maximum absorption wavelength; C and A are the concentration and absorbance of MO/MB solution at 464/664 nm during photocatalytic reaction.

Furthermore, we also tested the performance of the photocatalyst upon excitation with UV light by using another reactor system. The photocatalytic reactor consists of two parts, a quartz cell with a circulating water jack and a 500 W high-pressure mercury lamp with a maximum emission at 365 nm placed inside the quartz cell. The powders concentration in the MO or MB aqueous solution was also 0.20 g/100 mL. And the volume of initial MO or MB solution was 300 mL, with the concentration of 10 mg/L.

3. Results and discussion

3.1. Characterizations of the powders

The XRD patterns of the as-prepared samples are shown in Fig. 1. The samples of $PbBiO_2Br$, BiOBr, $BiOI_{0.8}Cl_{0.2}$, $PbBi_2Nb_2O_9$, and $TiO_{2-x}N_x$ all possess pure phases. And as shown in the figure, the crystal structure of the as-prepared sample $PbBiO_2Br$ did not change before and after the photocatalytic reaction. It indicates that $PbBiO_2Br$ can be used as a stable photocatalyst, which is one of the key factors for the practical use.

The UV–vis diffuse reflectance absorption spectra of the $PbBiO_2Br$, BiOBr, $BiOI_{0.8}Cl_{0.2}$, $PbBi_2Nb_2O_9$, and $TiO_{2-x}N_x$ samples are shown in Fig. 2. The $PbBiO_2Br$ sample shows an absorption band-edge of about 530 nm, and the red shift appears to be about

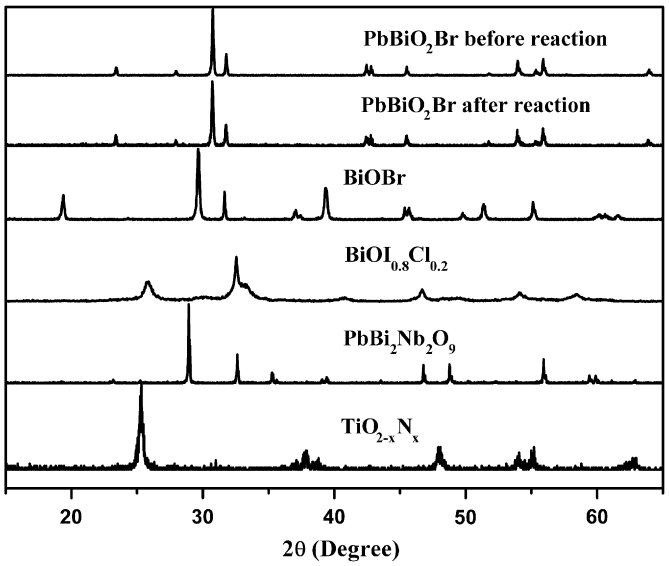

Fig. 1. XRD spectra of $PbBiO_2Br$ before and after the photocatalytic reaction, BiOBr, $BiOI_{0.8}Cl_{0.2}$, $PbBi_2Nb_2O_9$, and $TiO_{2-x}N_x$.

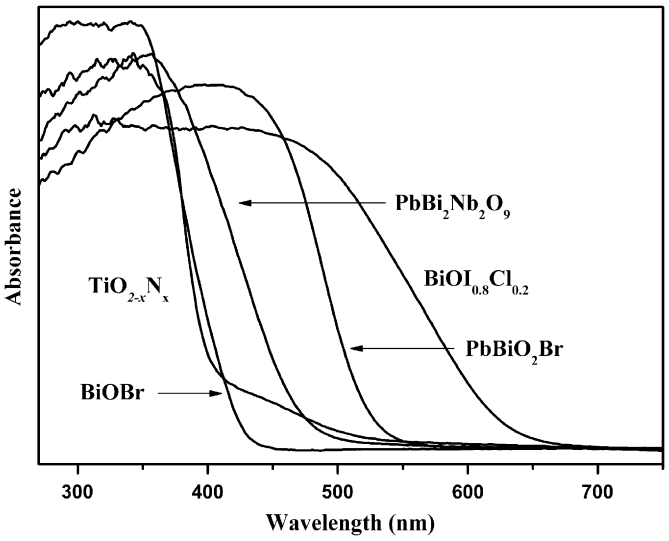

Fig. 2. UV–vis diffuse reflectance spectra of $PbBiO_2Br$, BiOBr, $BiOI_{0.8}Cl_{0.2}$, $PbBi_2Nb_2O_9$, and $TiO_{2-x}N_x$.

100 nm by the comparison with that of BiOBr. The bandgaps of $PbBiO_2Br$, BiOBr, $BiOI_{0.8}Cl_{0.2}$, $PbBi_2Nb_2O_9$, and $TiO_{2-x}N_x$ are 2.3, 2.9, 1.98, 2.6, and 2.88 eV, respectively. Except the red color of $BiOI_{0.8}Cl_{0.2}$, the others are yellow or yellowish, indicating that these materials indeed absorb visible light.

The typical morphologies of the initial $PbBiO_2Br$, BiOBr, $BiOI_{0.8}Cl_{0.2}$, $PbBi_2Nb_2O_9$, and $TiO_{2-x}N_x$ powders are demonstrated in Fig. 3. As displayed in the figure, BiOBr and $BiOI_{0.8}Cl_{0.2}$ are nano-sized particles, while $PbBiO_2Br$, $TiO_{2-x}N_x$, and $PbBi_2Nb_2O_9$ are micron-sized powders. In Fig. 3 (a) [16] and (b), the images of the $BiOI_{0.8}Cl_{0.2}$ and BiOBr samples are at magnification of 60,000 × and 50,000 ×, respectively. The images show that the products are composed of plates with a diameter of approximately 100 and 50 nm in thickness. In Fig. 3 (c), (d) and (e), the images of $PbBiO_2Br$, $TiO_{2-x}N_x$, and $PbBi_2Nb_2O_9$ powders are at the same magnification of 5000 ×. The morphology of $PbBiO_2Br$ is also plates just like the other oxyhalides, and the particles sizes are estimated to be about 1–3 μm, much lager than those of BiOBr and $BiOI_{0.8}Cl_{0.2}$. The morphology of $TiO_{2-x}N_x$ and $PbBi_2Nb_2O_9$ are both spheres, and the average particle sizes are about 1–2 and 2–4 μm, respectively.

3.2. Photodegradation of dyes

The visible-light-driven photocatalytic activities of $PbBiO_2Br$, BiOBr, $BiOI_{0.8}Cl_{0.2}$, $PbBi_2Nb_2O_9$, and $TiO_{2-x}N_x$ were observed under 8 h visible light irradiation ($\lambda > 420$ nm), at ambient temperature in air, as shown in Fig. 4. It is obvious that MO can be photocatalyzed by about 18%, 23%, and 38% on $TiO_{2-x}N_x$, $PbBi_2Nb_2O_9$, and BiOBr, respectively. The values are much lower than 95% on $PbBiO_2Br$. It is worth mentioning that the higher activity of $PbBi_2Nb_2O_9$ than $TiO_{2-x}N_x$ for dye degradation observed in this work is consistent with the conclusion in the water-splitting study reported by Kim and his coworkers [20]. As revealed in the figure, the activity for photocatalytic degradation of MO on $PbBiO_2Br$ was lower than that on $BiOI_{0.8}Cl_{0.2}$, where the complete photodecomposition was achieved within 5 h. The visible-light-response activity order, $BiOI_{0.8}Cl_{0.2} > PbBiO_2Br > BiOBr > PbBi_2Nb_2O_9 > TiO_{2-x}N_x$, can be also found in the degradation of MB.

The UV-assisted photocatalytic activities for decolorizing MO or MB are shown in Fig. 5. Dissimilar to the case of visible light irradiation, $PbBiO_2Br$ is only more photocatalytically active than $PbBi_2Nb_2O_9$, and less active than the other references (BiOBr, $BiOI_{0.8}Cl_{0.2}$, and $TiO_{2-x}N_x$) for MO and MB degradation under UV light. Taking MO degradation as an example, the dye can be completely degraded over $PbBiO_2Br$ during 60 min light irradiation, and the completely discoloring time over $BiOI_{0.8}Cl_{0.2}$, $TiO_{2-x}N_x$, and BiOBr are shortened to 30, 40, and 50 min, respectively. The least active semiconductor, $PbBi_2Nb_2O_9$, degrades only 25% MO within 60 min of photocatalytic reaction.

A larger band gap corresponds to a more powerful redox ability [28]. Because the photocatalytic process system can be considered to be similar to that of an electrochemical cell, a larger band gap results in an enhanced oxidation–reduction potential [29], and the effect is the same as the suppress reaction of the recombination of electron and hole pairs. Besides that, the light source and light absorption are very important for the performance of photocatalysts. For $PbBiO_2Br$ and $TiO_{2-x}N_x$, the band gaps are 2.3 eV (540 nm) and 2.88 eV (430 nm), respectively. Under visible light irradiation ($\lambda \geqslant 420$ nm), $PbBiO_2Br$, absorbing more visible light than $TiO_{2-x}N_x$, leads to the superior photocatalytic activity to $TiO_{2-x}N_x$. However, under UV light irradiation ($\lambda \leqslant 420$ nm), both $PbBiO_2Br$ and $TiO_{2-x}N_x$ can absorb all light. Under such situation, the intrinsic oxidation–reduction potential is the key factor for the photocatalytic activity. The band gap of $TiO_{2-x}N_x$ is larger than that of $PbBiO_2Br$. Naturally, its photocatalytic activity is higher than that of $PbBiO_2Br$. Furthermore, the inferior photocatalytic activity of $PbBiO_2Br$ to $BiOI_{0.8}Cl_{0.2}$ under visible light irradiation is mainly due to that $PbBiO_2Br$ possess much larger particle size than nano-sized $BiOI_{0.8}Cl_{0.2}$.

We have discussed dye degradation mechanisms in our previous work Bi_3O_4Cl [30]. There are three possible reaction mechanisms for the dye degradation in the previous experiments, including (1) a photocatalytic process, (2) a dye photosensitization process, and (3) a photolysis process. In our opinion, the oxyhalides should have the similar dyes bleaching mechanisms. Since MO and MB show high structural chemical stability, the photolysis of MO and MB can be neglected. In other words, the MO and MB degradation is resulted possibly from a photocatalytic process and a photosensitization process. Similar to Bi_3O_4Cl, the concentration decrease of MO and MB in the $PbBiO_2Br$ suspension

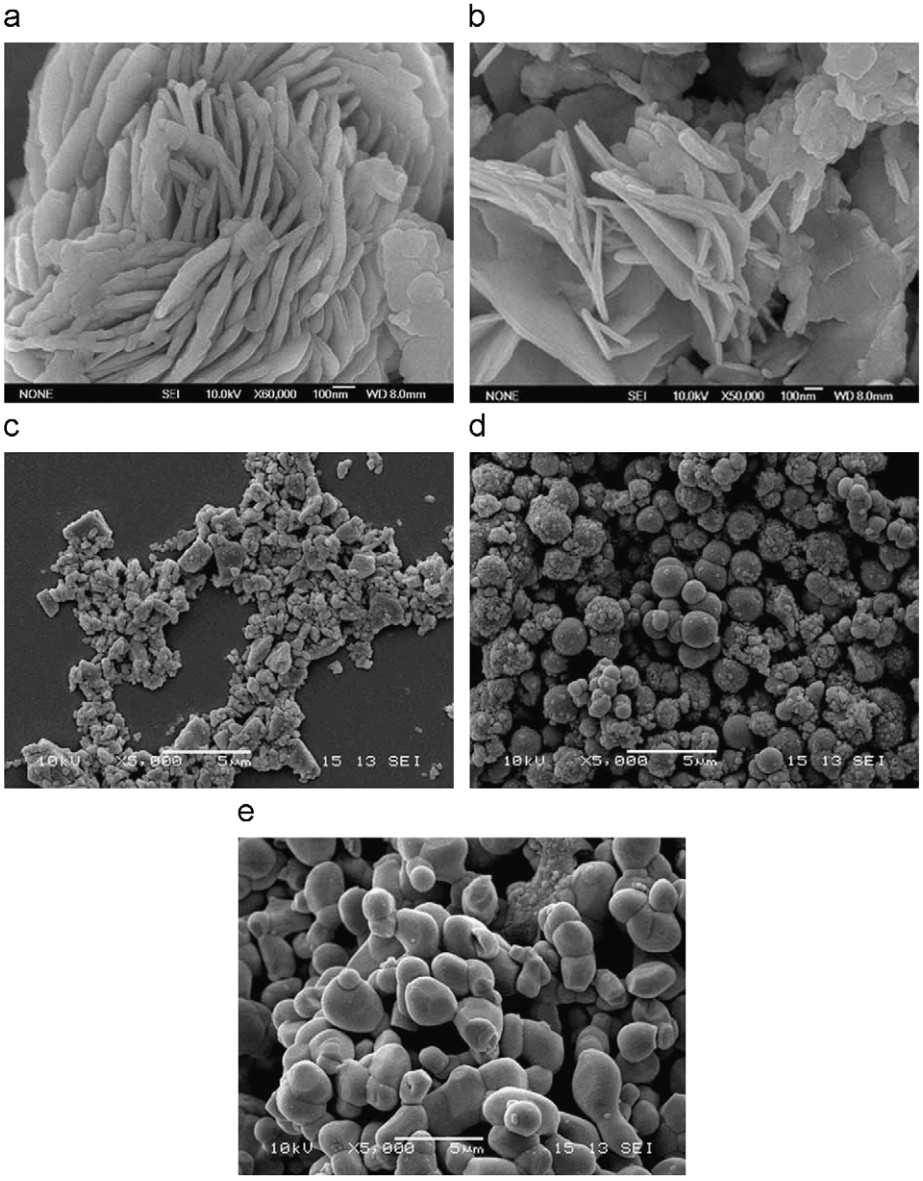

Fig. 3. SEM images of $BiOI_{0.8}Cl_{0.2}$, BiOBr, $PbBiO_2Br$, $TiO_{2-x}N_x$, and $PbBi_2Nb_2O_9$.

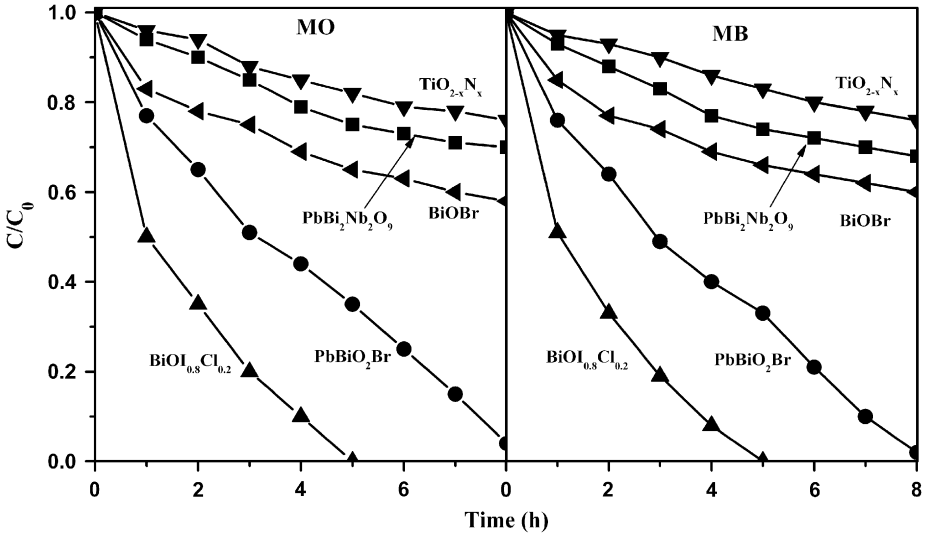

Fig. 4. MO and MB photodegradations under visible light irradiation.

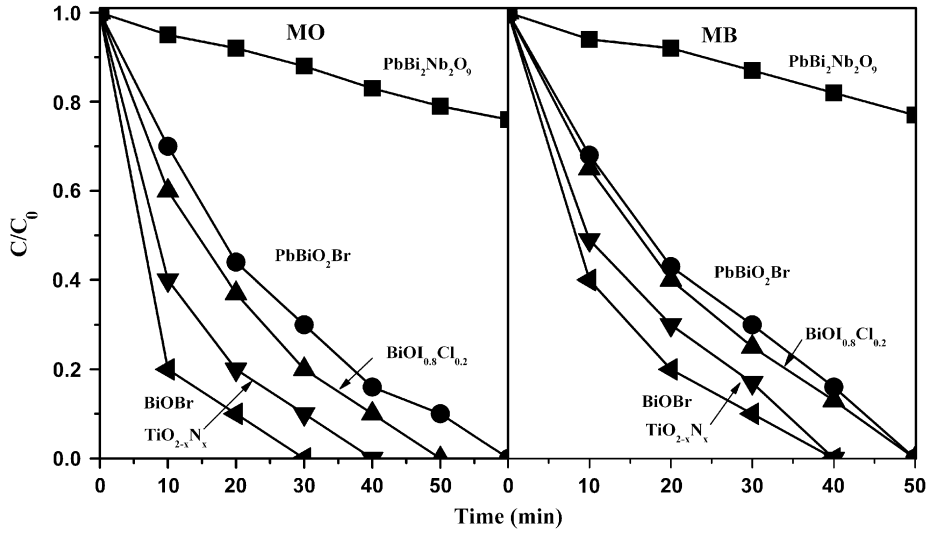

Fig. 5. MO and MB photodegradations under UV light irradiation.

should be ascribed to a photocatalytic process under irradiation of UV light or visible light.

3.3. Structure–property relationship

The layered structure $PbBiO_2Br$ crystallizes in the *I*4/*mmm* space group with a tetragonal lattice. Each oxygen atom is coordinated by four metal (*M*) atoms of two Pb and two Bi. The resulting edge-sharing OM_4 tetrahedra form the $[PbBiO_2]$ layers perpendicular to [001], connected by the intermediate Br atoms. Each metal atom is surrounded by four O and four Br atoms to form a tetragonal antiprism. The Br atom is coordinated to the tetragonal prism of eight metal atoms [31].

The photocatalytic oxidation of the organic contaminants is closely correlative to two factors: efficient photoinduced electron–hole separation and transfer and the structure of the band gap in the photocatalyst. In the process of photocatalytic degradation, charge separation is important and necessary to prevent recombination of the photoinduced electrons and holes. The internal electric fields are one of the important parameters to evaluate the ability of electron–hole separation and transport in the crystal lattice. Generally, the presence of internal electric fields between $[PbBiO_2]$ and $[Br_2]$ are favorable for the efficient photoinduced electron–hole separation and transfer, which is also propitious to a high-photocatalytic efficiency of $PbBiO_2Br$.

Band structure of $PbBiO_2Cl$ was calculated by TB-LMTO program [32]. From the calculated results of $PbBiO_2Cl$, the density of states of the analogue $PbBiO_2Br$ can be reasonably derived. The conduction band minimum (CBM) of the oxybromide should be mainly composed of Bi 6*p*, O 2*p*, Pb 6*p*, Br 4*p* states, and the valence band maximum (VBM) primarily consists of Br 4*p*, O 2*p*, and Pb 6*s* orbitals. The rather hybrid bonding and antibonding states of Pb/Bi O/Br bonds are distributed around the top of valance band and the bottom of conduction band. The DOS distribution near CBM and VBM becomes broader than BiOBr, BiOCl, and $PbBiO_2Cl$ due to the hybridization of the Pb and Br valence orbitals, which increases the mobility of photo-generated hole. Fig. 6 shows the schematic band gaps of BiOCl, BiOBr, $PbBiO_2Cl$, and $PbBiO_2Br$.

The much dispersed states near the forbidden band in $PbBiO_2Br$ are believed to enable the photo-induced electrons and holes to travel a long distance and the internal electric fields between $[PbBiO_2]$ and $[Br_2]$ slabs, assisting a high mobility for the separation of electron–hole pairs and consequently improving the photocatalytic activity.

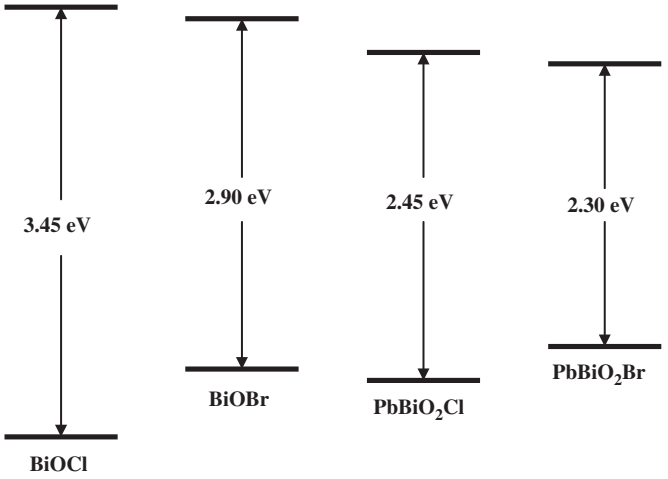

Fig. 6. Schematic band gaps of BiOCl, BiOBr, $PbBiO_2Cl$, and $PbBiO_2Br$.

4. Conclusions

In conclusion, the photocatalyst $PbBiO_2Br$ with a layered structure synthesized by a solid-state reaction method has an intrinsic optical band gap of 2.3 eV. The material possesses high higher photocatalytic activities for degrading MO and MB both under UV and visible light. The high activity is closely related with the internal electric fields between $[PbBiO_2]$ and $[Br_2]$ slabs, as well as the hybrid states at the conduction and valence bands.

Acknowledgments

This research was financially supported by National 973 Program of China Grant 2007CB936704, National Science Foundation of China Grant 50772123, Science and Technology Commission of Shanghai Grant 0752nm016 and Excellent Young Teachers Program of MOE.

References

[1] K. Honda, A. Fujishima, Nature 238 (1972) 37.
[2] R. Asahi, T. Morikawa, T. Ohwaki, K. Aoki, Y. Taga, Science 293 (2001) 269.
[3] Z. Zou, J. Ye, K. Sayama, H. Arakawa, Nature 414 (2001) 625.
[4] A.L. Linsebigler, G. Lu, J.T. Yates, Chem. Rev. 95 (1995) 735.
[5] W. Ma, J. Li, X. Tao, J. He, Y. Xu, J.C. Yu, J. Zhao, Angew. Chem. Int. Ed. 42 (2003) 1029.
[6] J. Sato, N. Saito, Y. Yamada, K. Maeda, T. Takata, J.N. Kondo, M. Hara, H. Kobayashi, K. Domen, Y. Inoue, J. Am. Chem. Soc. 127 (2005) 4150.
[7] K. Maeda, K. Teramura, D. Lu, T. Takata, N. Saito, Y. Inoue, K. Domen, Nature 440 (2006) 295.
[8] J. Tang, Z. Zou, J. Ye, J. Phys. Chem. B 107 (2003) 14265.
[9] M. Machida, J. Yabunaka, T. Kijima, Chem. Mater. 12 (2000) 812.
[10] D. Hwang, J.S. Lee, W. Li, S.H. Oh, J. Phys. Chem. B 107 (2003) 4963.
[11] S. Ouyang, H. Zhang, D. Li, T. Yu, J. Ye, Z. Zou, J. Phys. Chem. B 110 (2006) 11677.
[12] W. Yao, J. Ye, Chem. Phys. Lett. 435 (2007) 96.
[13] S. Matsushimaa, K. Obataa, H. Nakamurab, M. Araic, K. Kobayashid, J. Phys. Chem. Solids 64 (2003) 2417.
[14] K.L. Zhang, C.M. Liu, F.Q. Huang, C. Zheng, W.D. Wang, Appl. Catal. B 68 (2006) 125.
[15] W.D. Wang, F.Q. Huang, X.P. Lin, J.H. Yang, Catal. Commun. 9 (2008) 8.
[16] W.D. Wang, F.Q. Huang, X.P. Lin, Scripta Mater. 56 (2007) 669.
[17] X.P. Lin, F.Q. Huang, W.D. Wang, K.L. Zhang, Appl. Catal. A 307 (2006) 257.
[18] W.F. Yao, X.H. Xu, H. Wang, J.T. Zhou, X.N. Yang, Y. Zhang, S.X. Shang, B.B. Huang, Appl. Catal. B 52 (2004) 109.
[19] H. Kato, H. Kobayashi, A. Kudo, J. Phys. Chem. B 106 (2002) 12441.
[20] H. Kim, D.W. Hwang, J.S. Lee, J. Am. Chem. Soc. 126 (2004) 8912.
[21] A. Kudo, K. Omori, H. Kato, J. Am. Chem. Soc. 121 (1999) 11459.
[22] R. Asahi, T. Morikawa, T. Ohwaki, K. Aoki, Y. Tao, Science 293 (2001) 269.
[23] T. Ohno, M. Akiyoshi, T. Umebayashi, K. Asai, T. Mitsui, M. Matsumura, Appl. Catal. A 256 (2004) 115.
[24] M. Yan, F. Chen, J. Zhang, M. Anpo, J. Phys. Chem. B 109 (2005) 8673.
[25] X. Lin, F. Huang, W. Wang, Y. Wang, Y. Xia, J. Shi, Appl. Catal. A 313 (2006) 218.
[26] J. Lin, J.C. Yu, D. Lo, S.K. Lam, J. Catal. 183 (1999) 368.
[27] Y. Yu, J.C. Yu, J.G. Yu, Y.C. Kwo, Y.K. Che, J.C. Zhao, L. Ding, W.K. Ge, P.K. Wong, Appl. Catal. A 289 (2005) 186–196.
[28] J.C. Yu, L. Zhang, J. Yu, Chem. Mater. 14 (2002) 4647.
[29] M.R. Hoffmann, S.T. Martin, W. Choi, et al., Chem. Rev. 95 (1995) 69.
[30] X. Lin, T. Huang, F. Huang, W. Wang, J. Shi, J. Phys. Chem. B 110 (2006) 24629.
[31] J. Ketterer, V. Kramer, Mat. Res. Bull. 20 (1985) 1031.
[32] Unpublished data.